First-principles investigation on Cu/ZnO catalyst precursor: Energetic, structural and electronic properties of Zn-doped $Cu_2(OH)_2CO_3$

ARTICLE *in* COMPUTATIONAL MATERIALS SCIENCE · JANUARY 2015

Impact Factor: 2.13 · DOI: 10.1016/j.commatsci.2014.08.038

4 AUTHORS, INCLUDING:

Huayan Zheng
Taiyuan University of Technology
17 PUBLICATIONS **111** CITATIONS
SEE PROFILE

Xiaochao Zhang
Taiyuan University of Technology
26 PUBLICATIONS **185** CITATIONS
SEE PROFILE

Computational Materials Science 96 (2015) 1–9

Contents lists available at ScienceDirect

Computational Materials Science

journal homepage: www.elsevier.com/locate/commatsci

First-principles investigation on Cu/ZnO catalyst precursor: Energetic, structural and electronic properties of Zn-doped $Cu_2(OH)_2CO_3$

Jiao Li [a], Huayan Zheng [a,*], Xiaochao Zhang [b], Zhong Li [a,*]

[a] Key Laboratory of Coal Science and Technology of Ministry of Education and Shanxi Province, Taiyuan University of Technology, Taiyuan 030024, Shanxi, China
[b] Institute of Clean Technique for Chemical Engineering, Taiyuan University of Technology, Taiyuan 030024, Shanxi, China

ARTICLE INFO

Article history:
Received 18 May 2014
Received in revised form 25 July 2014
Accepted 22 August 2014
Available online 20 September 2014

Keywords:
Zn-doped $Cu_2(OH)_2CO_3$
First-principles
Formation energy
Jahn–Teller effect
Electronic structures

ABSTRACT

First-principles calculations are performed to investigate the energetic, structural and electronic properties of $(Cu_{1-x}Zn_x)_2(OH)_2CO_3$ (x = 0, 1/8, 2/8, 3/8 and 4/8) crystals usually as Cu/ZnO catalyst precursor for methanol synthesis. The calculation results show that $(Cu_{6/8}Zn_{2/8})_2(OH)_2CO_3$, exhibiting the weakest Jahn–Teller distortion, is the most stable structure in thermodynamics due to the lowest formation energy. Meanwhile, Zn atoms are preferentially located on the Cu_2 sites, in good agreement with the crystal field theory. The calculated structural parameters, including the equilibrium lattice constants and average bond lengths, are consistent with the available experimental results. The analysis results of Mulliken charges, bond populations, charge density difference and density of states demonstrate that covalent feature of Zn–O bonds are much stronger than Cu–O bonds, and covalent features gradually enhance in Zn-doped $Cu_2(OH)_2CO_3$ system with the incorporation amount of Zn dopant increasing. The lowest peak value of valence electrons of $(Cu_{6/8}Zn_{2/8})_2(OH)_2CO_3$ at the Fermi level further implies the most stable structure. Our computational results of $(Cu_{1-x}Zn_x)_2(OH)_2CO_3$ precursors should provide the fundamental and meaningful theoretical guidance for understanding and preparing the highly active Cu/ZnO catalyst.

1. Introduction

Synthetic mixed Cu/Zn hydroxycarbonate materials, as catalyst precursors of Cu/ZnO, have been paid particular attention to the industrial methanol synthesis [1–3]. It is well-known that the microstructure, physicochemical properties and catalytic performance of Cu/ZnO catalyst significantly depends on the physical structure and the nature of precursor material [4–9]. Experimental results have demonstrated the role of precursor composition for the Cu dispersion in the final catalyst. The properties of Cu/ZnO catalysts can be easily traced back to the phase-pure precursor compounds. Zn-doped malachite, one type of mixed Cu, Zn hydroxide carbonates, is the primary phase for the preparation of nano-structure Cu/ZnO-based catalyst which is expected to exhibit a higher dispersion of the catalytically active copper phase because of the efficient stabilizing function of ZnO phase [10,11]. The incorporation of Zn^{2+} into the cationic lattice of malachite favors the nanostructuring of the Cu/ZnO catalyst owing to the perfect distribution of both species in the joint crystal lattice of the precursor compound. This can be understood as a purely geometric effect [4]. Therefore, it is highly desirable for the optimization of catalyst precursors to investigate the possibilities of Cu/Zn substitution in malachite and further understand comprehensively the associated properties of Zn-doped malachite.

Malachite, the monoclinic crystal structure with the formula $Cu_2(OH)_2CO_3$, is composed of octahedral CuO_6 building blocks interconnected by carbonate groups [12]. Two structurally distinct copper sites, Cu_1 and Cu_2, are present in a 1:1 ratio. Due to Jahn–Teller effect [13], both sites are equatorially surrounded by four oxygen atoms at the shorter distances and two ones at the longer distances in axial arrangement [14].

Zn-doped malachite, $(Cu_{1-x}Zn_x)_2(OH)_2CO_3$, is prepared by pseudo-isomorphous substitution series of Zn^{2+} into $Cu_2(OH)_2CO_3$. The maximum value with $x \approx 0.27$ has been rather outstanding achievement for state-of-the-art catalysts in the previous literatures [15,16], and attempt to further achieve the Zn content near x = 0.5, as high as in natural rosasite $(Cu, Zn)_2(OH)_2CO_3$ [11], has been a formidable challenge. Because the increasing Zn content leads to the phase mixtures containing Zn-doped malachite with low Zn content and the more zinc-rich mixed hydroxide carbonate, $(Zn, Cu)_5(OH)_6(CO_3)_2$ [10,11,15,17,18]. In addition, Zn^{2+} ions in the

* Corresponding authors. Address: No. 79 Yingze West Street, Taiyuan 030024, China. Tel./fax: +86 351 6018526.
E-mail addresses: zhenghuayan@tyut.edu.cn (H. Zheng), lizhong@tyut.edu.cn (Z. Li).

http://dx.doi.org/10.1016/j.commatsci.2014.08.038
0927-0256/

zinc malachite phase are preferentially located on the Cu_2 sites, which has been demonstrated in previous experiments on the basis of Ultraviolet–visible–Near Infrared Reflection (UV–vis–NIR) spectra [12] and X-ray diffraction (XRD) [15]. Such a zinc ordering on the Cu_2 site is also expected from crystal field considerations, because Cu_2 site is in a less distorted environment than Cu_1 site in pure malachite and thus more suited for the coordination requirements of Zn^{2+}. However, it is difficult to provide a direct access to the distribution of Cu and Zn for two available metal sites in the malachite structure using the laboratory approaches, but certain sites need be deduced indirectly from the average distortion of the MO_6 (M = Cu, Zn) coordination polyhedra, and the involved micro-structure molecular level analysis and theoretical reasons for the upper limit level of x in synthetic $(Cu_{1-x}Zn_x)_2(OH)_2CO_3$ have been indistinct in the previous literatures. Recently, first-principles calculations based on density functional theory (DFT) have been adopted to become a very powerful tool for obtaining microscopic insights into structural properties of catalytic materials. At present, the magnetic properties of malachite have been investigated based on DFT [19], but there is little information on the Zn doping malachite system using first-principles calculations. Here, the aim of this study is to provide fundamental information on the physical structure and the nature of $(Cu_{1-x}Zn_x)_2(OH)_2CO_3$, such as, the determination of the most stable structure among various Zn-doped malachite and the preferential substitution sites of Zn.

In this work, the first-principles calculation has been performed to investigate the effect of various Zn-doping levels on the energetic, structural and electronic properties of $Cu_2(OH)_2CO_3$. The fully relaxed lattices of various possible $(Cu_{1-x}Zn_x)_2(OH)_2CO_3$ (x = 1/8, 2/8, 3/8 and 4/8) compounds are calculated to yield the lowest energy configurations. Based on the most stable configurations at different Zn content levels, we systematically discuss the structural and electronic properties consisting of Mulliken charges, bond populations and densities of states. The obtained results could further provide the fundamental and significative theoretical guidance for understanding and preparing the highly-activity Cu/ZnO catalyst.

2. Computational details

2.1. Computational models

Malachite crystallizes in the monoclinic space group $P2_1/a$ with lattice parameters, a = 9.502, b = 11.974, c = 3.240 Å and β = 98.75° (Z = 4) [20–22]. The experimental structure of malachite is used as the initial configuration in the calculations. Fig. 1 illustrates the structure model of $Cu_2(OH)_2CO_3$ unit cell. In the geometry optimization cell, there exist eight Cu positions for Zn substitution: four Cu_1 positions (labeled 1, 2, 3, 4) and four Cu_2 positions (marked 5, 6, 7, 8), as listed in Fig. 1. The Zn-doped $Cu_2(OH)_2CO_3$ systems are conducted by replacing one, two, three and four Cu atoms corresponding to Zn-doping level of 12.5%, 25%, 37.5% and 50%, respectively. Namely, the values of x in $(Cu_{1-x}Zn_x)_2(OH)_2CO_3$ are 1/8, 2/8, 3/8 and 4/8. The models of $(Cu_{7/8}Zn_{1/8})_2(OH)_2CO_3$ are obtained by replacing one Cu atom with an Zn atom at 1, 3, 5 or 7 site. For $(Cu_{6/8}Zn_{2/8})_2(OH)_2CO_3$, there are three configurations of Zn atoms replacing Cu atoms, including 1, 2 sites ($2Cu_1$), or 1, 6 sites ($Cu_1 + Cu_2$), or 5, 6 sites ($2Cu_2$). For $(Cu_{5/8}Zn_{3/8})_2(OH)_2CO_3$, three Zn atoms are introduced to $3Cu_1$, $2Cu_1 + Cu_2$, $Cu_1 + 2Cu_2$ and $3Cu_2$ sites. Similarly, four Zn atoms are replaced at the $4Cu_1$, $3Cu_1 + Cu_2$, $2Cu_1 + 2Cu_2$, $Cu_1 + 3Cu_2$ and $4Cu_2$ sites in the models of $(Cu_{4/8}Zn_{4/8})_2(OH)_2CO_3$.

2.2. Computational methods

First-principles calculation has been performed using the well-tested Cambridge Serial Total Energy Package (CASTEP) code [23,24] based on DFT, which includes the ultrasoft pseudopotentials [25], the periodic boundary conditions, the k-point sampling techniques and the Broyden–Fletcher–Goldfarb–Shanno (BFGS) scheme for geometry optimization. The Local Density Approximation (LDA) [26] was used for the exchange–correlation potential. The computational details were itemized as follows: SCF tolerance was set at 1.0×10^{-6} eV/atom, energy cutoff was 380 eV, k-point of Brillouin zone was $3 \times 2 \times 8$. The convergence thresholds between geometry optimization cycles for energy change, maximum force, maximum stress and maximum displacement were 1×10^{-5} eV/atom, 0.05 eV/Å, 0.05 GPa and 0.001 Å, respectively. The considered valence configurations were $2s^22p^2$, $2s^22p^4$, $3d^{10}4s^1$, and $3d^{10}4s^2$ for C, O, Cu, and Zn, respectively. In addition, the formation energy, charge density difference and electronic density of states were investigated based on the relaxed crystal structures.

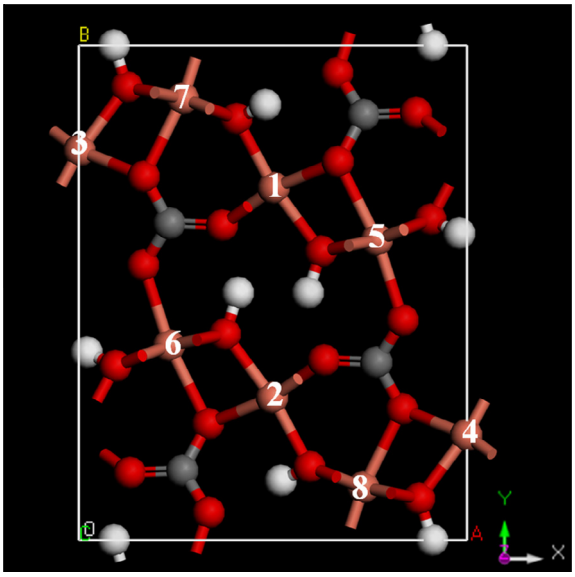

Fig. 1. The optimized structure of malachite unit cell in which the Zn atoms can be doped at 1, 2, 3, 4, 5, 6, 7 and 8 sites representing other configurations. Cu, O, C and H atoms are described by orange, red, gray and white spheres, respectively. (For interpretation of the references to color in this figure legend, the reader is referred to the web version of this article.)

3. Results and discussion

3.1. Formation energy and stability

To examine the structural stability of $(Cu_{1-x}Zn_x)_2(OH)_2CO_3$, the formation energies of $Cu_2(OH)_2CO_3$ doped with various Zn contents were calculated according to the following formulas [27–29],

$$E_f = [E_{tot}(\text{doped}) + nE_{Cu} - E_{tot}(\text{pure}) - nE_{Zn}]/n$$

where E_{tot}(pure) and E_{tot}(doped) are the total energies of $Cu_2(OH)_2CO_3$ and Zn doping $Cu_2(OH)_2CO_3$ system. E_{Cu} and E_{Zn} represent the chemical potential of Cu and Zn atoms calculated from the bulk metal materials, respectively. n corresponds to the number of Zn atoms replacing Cu in the lattice of $Cu_2(OH)_2CO_3$.

The calculated formation energies and total energies for various types of $(Cu_{1-x}Zn_x)_2(OH)_2CO_3$ (x = 0, 1/8, 2/8, 3/8 and 4/8) have been presented in Table 1. The results indicate that the formation energies of Zn-doped $Cu_2(OH)_2CO_3$ system are more positive than that of pure $Cu_2(OH)_2CO_3$, suggesting that the stability of $(Cu_{1-x}Zn_x)_2(OH)_2CO_3$ should become more poor than pure $Cu_2(OH)_2CO_3$ in the experiment. For x = 1/8, the formation energy of Zn substitution at the site 5 (Cu_2 site) is the lowest (0.712 eV) among the four possible sites (marked 1, 3, 5, 7 in Fig. 1), which is 25.4% lower than

Table 1
Total energies (E_{tot}) and formation energies (E_f) of $(Cu_{1-x}Zn_x)_2(OH)_2CO_3$ compounds calculated for different number of substituted atoms. The substitution site labels correspond to those given in Fig. 1.

System	Substitution site		E_{tot} (eV)	E_f (eV)
$Cu_2(OH)_2CO_3$	–		−20270.093	0
$(Cu_{7/8}Zn_{1/8})_2(OH)_2CO_3$	Cu_1	1	−20634.914	0.954
		3	−20634.922	0.946
	Cu_2	5	−20635.156	0.712(E_{min})
		7	−20635.153	0.715
$(Cu_{6/8}Zn_{2/8})_2(OH)_2CO_3$	$2Cu_1$	1, 2	−20999.838	0.902
	$Cu_1 + Cu_2$	1, 6	−20999.977	0.833
	$2Cu_2$	5, 6	−21000.237	0.703(E_{min})
$(Cu_{5/8}Zn_{3/8})_2(OH)_2CO_3$	$3Cu_1$	1, 2, 3	−21364.706	0.904
	$2Cu_1 + Cu_2$	1, 2, 5	−21365.036	0.794
	$Cu_1 + 2Cu_2$	1, 5, 6	−21365.208	0.737
	$3Cu_2$	5, 6, 7	−21365.259	0.720(E_{min})
$(Cu_{4/8}Zn_{4/8})_2(OH)_2CO_3$	$4Cu_1$	1, 2, 3, 4	−21729.188	1.001
	$3Cu_1 + Cu_2$	1, 2, 3, 5	−21729.990	0.801
	$2Cu_1 + 2Cu_2$	1, 2, 5, 6	−21730.283	0.727
	$Cu_1 + 3Cu_2$	1, 5, 6, 8	−21730.271	0.730
	$4Cu_2$	5, 6, 7, 8	−21730.292	0.725(E_{min})

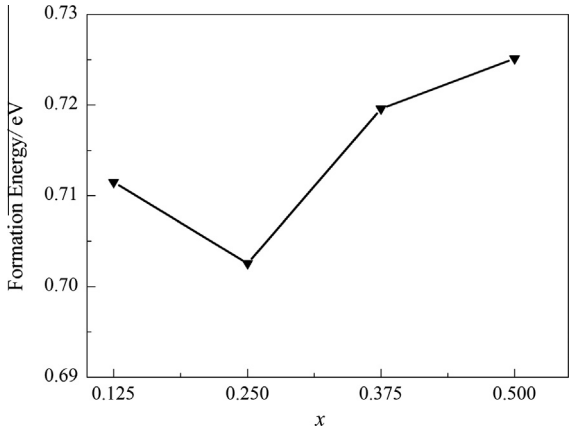

Fig. 2. The calculated minimum formation energy (E_f) for $(Cu_{1-x}Zn_x)_2(OH)_2CO_3$ (x = 1/8, 2/8, 3/8 and 4/8).

the highest formation energy (0.954 eV) of Zn doping at site 1 (Cu_1 site). Similarly, for $(Cu_{1-x}Zn_x)_2(OH)_2CO_3$ (x = 2/8, 3/8 and 4/8), the supercells with Zn replacing Cu_2 sites also lead to the lowest formation energy, whereas the configurations with Zn doping Cu_1 sites obtain the maximum values, as listed in Table 1. As a result, Zn atoms would be favorable in the Cu_2 sites for Zn-doped malachite unit cell, which is in good agreement with the experimental results [12,15,30]. Moreover, based on crystal field theory, the Zn^{2+} ion has a completely filled electronic $3d^{10}$ shell, resulting in the less distorted octahedral coordination. The Cu_2O_6 is the initially less distorted polyhedron than Cu_1O_6 octahedron in pure malachite and thus more suitable for the coordination requirements of Zn. In the following parts, only the correlative properties of the configurations with Zn substitution at Cu_2 sites (the most stable configurations) should be discussed in detail.

Fig. 2 gives the calculated minimum formation energies (E_f) for $(Cu_{1-x}Zn_x)_2(OH)_2CO_3$ (x = 1/8, 2/8, 3/8 and 4/8). It can be found that the formation energy of $(Cu_{6/8}Zn_{2/8})_2(OH)_2CO_3$ is the lowest, 0.703 eV, demonstrating that it is the most stable structure in thermodynamics for $(Cu_{1-x}Zn_x)_2(OH)_2CO_3$. Furthermore, the theoretical calculations agree with the previous experimental results that the maximum zinc content in $(Cu_{1-x}Zn_x)_2(OH)_2CO_3$ is estimated to be $x \approx 0.27$–0.28 [15,16]. With Zn content increasing, the formation energies of $(Cu_{1-x}Zn_x)_2(OH)_2CO_3$ increase, implying that the structure of materials become more unstable.

The variation trend of E_f may be relevant to the Jahn–Teller effect and the effects of the local charge density change. It is well known that in $Cu_2(OH)_2CO_3$, Cu_1 atom forms 6 bonds to adjacent oxygen atoms which belong to four carbonate ions and two hydroxyl ions, while Cu_2 atom is bonded to 6 oxygen atoms deriving from two carbonate ions and four hydroxyl ions, and Cu^{2+} shows the Jahn–Teller effect significantly in the six-coordination environment. The previous researches [31–33] have reported that introducing Zn^{2+} into hydrotalcite-like compounds containing Cu^{2+} could reduce the distortions of octahedrons resulting from Jahn–Teller effect, and bring about the formation of the more energetically favorable LDHs (layered double hydroxides). Ni et al. [34] have also addressed that the increasing Jahn–Teller effect would result in the poor stability of Cu–Zn–Al–LDHs. Hence, with the increase of Zn concentration, the diminishing formation energies of Zn-doped malachite system are likely to be caused by the weakening Jahn–Teller effect. On the other hand, to some extent, the existing Cu–O–Zn linkages affect the local charge density in the Zn-doped malachite system, leading to the increase of formation energy with the zinc content increasing. From this perspective, it

Table 2
Calculated lattice parameters for $(Cu_{1-x}Zn_x)_2(OH)_2CO_3$ system.

System	Lattice parameters (Å)			Cell angles (°)			V (Å^3)
	a	b	c	α	β	γ	
Experiments [20,21]	9.502	11.974	3.240	90.00	98.75	90.00	364.347
$Cu_2(OH)_2CO_3$	9.412	12.085	3.133	89.98	99.60	90.06	351.324
$(Cu_{7/8}Zn_{1/8})_2(OH)_2CO_3$	9.476	12.096	3.115	89.46	99.87	90.59	351.744
$(Cu_{6/8}Zn_{2/8})_2(OH)_2CO_3$	9.491	12.080	3.115	89.42	99.53	90.51	352.124
$(Cu_{5/8}Zn_{3/8})_2(OH)_2CO_3$	9.508	12.137	3.099	89.69	100.20	90.22	351.972
$(Cu_{4/8}Zn_{4/8})_2(OH)_2CO_3$	9.467	12.183	3.087	89.95	99.77	90.04	350.847

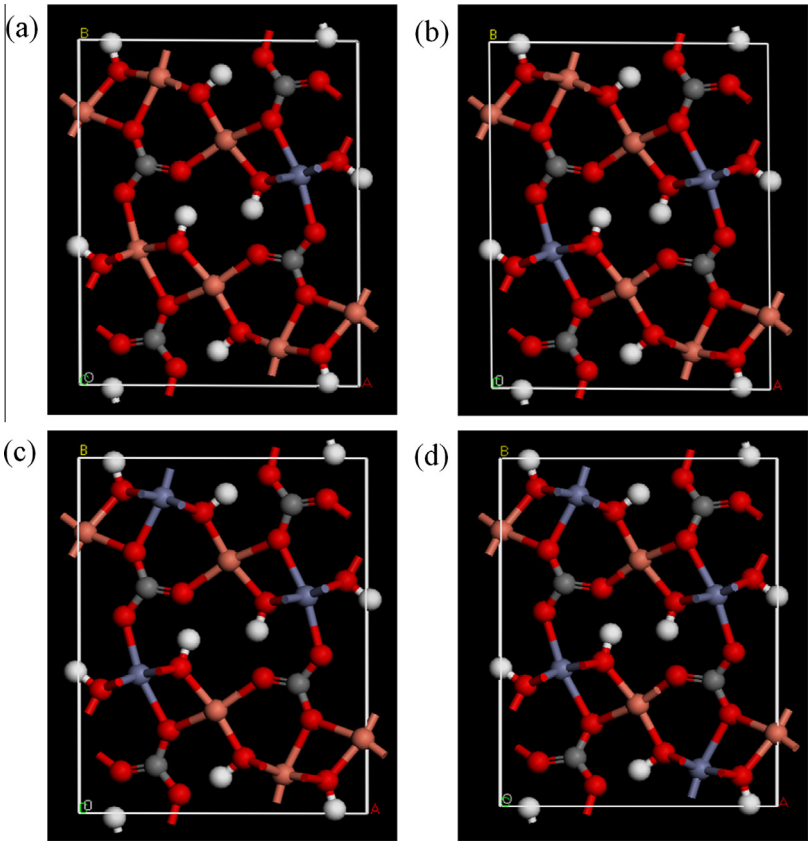

Fig. 3. Most stable configurations of the 40-atom $(Cu_{1-x}Zn_x)_2(OH)_2CO_3$ (x = 1/8, 2/8, 3/8 and 4/8) supercells. Zn, Cu, O, C and H atoms are described by blue, orange, red, gray and white spheres, respectively. (For interpretation of the references to color in this figure legend, the reader is referred to the web version of this article.)

can be concluded that the stability of $(Cu_{1-x}Zn_x)_2(OH)_2CO_3$ unit cell weakens with the increase in Cu–O–Zn bond number, similar to Yan et al. [35] reported who believe that the avoidance of Al–O–Al linkages is necessary for the stability of the Mg–Al layered double hydroxides (LDHs) structure. So the existence of the most unstable compound, $(Cu_{4/8}Zn_{4/8})_2(OH)_2CO_3$, is most probably the increasing concentration of Cu–O–Zn linkages, which destabilize the balanced charge density distribution in pure malachite. Besides, the larger ionic radius of Zn^{2+} (0.74 Å) compared with Cu^{2+} (0.72 Å) [36] may slightly give rise to the increase of formation energies of Zn-doped malachite system. Thus, taking various factors into account, the configuration of $(Cu_{6/8}Zn_{2/8})_2(OH)_2CO_3$ is the most stable structure.

3.2. Structural properties

Geometry optimization for $Cu_2(OH)_2CO_3$ crystal (conventional cell, 40 atoms) has been performed to obtain the equilibrium crystal structure. After relaxation, the cell parameters, a = 9.412; b = 12.085; c = 3.133 Å, are close to their experimental values (see Table 2), and the deviations between the simulated values and experimental ones [21] are within 1%. In this work, we have conducted an exhaustive search at different levels of Zn concentration, x, from 1/8 to 4/8 to determine the most stable structures of the $(Cu_{1-x}Zn_x)_2(OH)_2CO_3$ supercells, displayed in Fig. 3. The comparison between the equilibrium lattice constants of $(Cu_{1-x}Zn_x)_2(OH)_2CO_3$ are summarized in Table 2. There are variations in the lattice parameters, and a slight structure distortion occurs after the replacement of Zn. But the Zn-doped $Cu_2(OH)_2CO_3$ system displays similar structural symmetry, and apparently belongs to monoclinic structure. The constant b is determined by the equatorial M–O (M = Cu or Zn) bonds, which manifests an increasing trend as a whole. The decrease in the c parameter, from 3.133 to 3.087 Å, can be attributed to an augmentation of interlayer interaction. These phenomena are approximately agreement with experiment results [15]. The unsteady variation trend of lattice parameters, especially the constant a and monoclinic angle β may be due to the different number of Cu–O–Zn linkages and the symmetry between each other (see

Table 3
Average bond lengths and overlap populations (e) of $(Cu_{1-x}Zn_x)_2(OH)_2CO_3$ (x = 0, 1/8, 2/8, 3/8 and 4/8).

System	Cu_1–O			Cu_2–O			Zn–O		
	Population	Bond length (Å)		Population	Bond length (Å)		Population	Bond length (Å)	
		Equatorial	Apical		Equatorial	Apical		Equatorial	Apical
Experiment [21]	–	1.965	2.575	–	1.998	2.371	–	–	–
$Cu_2(OH)_2CO_3$	0.25	1.921	2.689	0.26	1.974	2.341	–	–	–
$(Cu_{7/8}Zn_{1/8})_2(OH)_2CO_3$	0.26	1.917	2.700	–	–	–	0.29	2.056	2.134
$(Cu_{6/8}Zn_{2/8})_2(OH)_2CO_3$	0.27	1.914	2.670	–	–	–	0.30	2.063	2.131
$(Cu_{5/8}Zn_{3/8})_2(OH)_2CO_3$	0.27	1.934	2.814	–	–	–	0.30	2.050	2.154
$(Cu_{4/8}Zn_{4/8})_2(OH)_2CO_3$	0.28	1.931	2.760	–	–	–	0.30	2.041	2.145

Table 4
The calculated atomic Mulliken charges (e) for ($\bar{2}01$) plane of $(Cu_{1-x}Zn_x)_2(OH)_2CO_3$ crystals (x = 0, 1/8, 2/8, 3/8 and 4/8).

System	Species	s	p	d	Total	Charge (e)
$Cu_2(OH)_2CO_3$	Cu_1	0.46	0.27	9.44	10.17	0.83
	Cu_2	0.45	0.28	9.41	10.14	0.86
	O_1	1.80	4.73	0	6.53	−0.53
	O_2	1.84	4.88	0	6.72	−0.72
	O_3	1.85	4.87	0	6.71	−0.71
	O_4	1.78	4.78	0	6.56	−0.56
	C	0.93	2.45	0	3.38	0.62
$(Cu_{7/8}Zn_{1/8})_2(OH)_2CO_3$	Cu_1	0.48	0.31	9.44	10.23	0.77
	Zn	0.12	0.53	9.98	10.63	1.37
	O_1	1.78	4.78	0	6.56	−0.56
	O_2	1.83	4.95	0	6.78	−0.78
	O_3	1.83	4.95	0	6.79	−0.79
	O_4	1.78	4.80	0	6.58	−0.58
	C	0.87	2.45	0	3.32	0.68
$(Cu_{6/8}Zn_{2/8})_2(OH)_2CO_3$	Cu_1	0.49	0.34	9.42	10.25	0.75
	Zn	0.14	0.56	9.98	10.68	1.32
	O_1	1.78	4.78	0	6.56	−0.56
	O_2	1.83	4.95	0	6.78	−0.78
	O_3	1.83	4.95	0	6.78	−0.78
	O_4	1.78	4.80	0	6.59	−0.59
	C	0.87	2.45	0	3.32	0.68
$(Cu_{5/8}Zn_{3/8})_2(OH)_2CO_3$	Cu_1	0.51	0.36	9.45	10.32	0.68
	Zn	0.16	0.57	9.98	10.71	1.29
	O_1	1.78	4.78	0	6.56	−0.56
	O_2	1.83	4.94	0	6.77	−0.77
	O_3	1.83	4.95	0	6.78	−0.78
	O_4	1.78	4.80	0	6.58	−0.58
	C	0.88	2.46	0	3.34	0.66
$(Cu_{4/8}Zn_{4/8})_2(OH)_2CO_3$	Cu_1	0.51	0.39	9.43	10.33	0.67
	Zn	0.18	0.60	9.98	10.76	1.24
	O_1	1.78	4.78	0	6.56	−0.56
	O_2	1.83	4.94	0	6.77	−0.77
	O_3	1.83	4.94	0	6.77	−0.77
	O_4	1.78	4.80	0	6.58	−0.58
	C	0.89	2.46	0	3.35	0.65

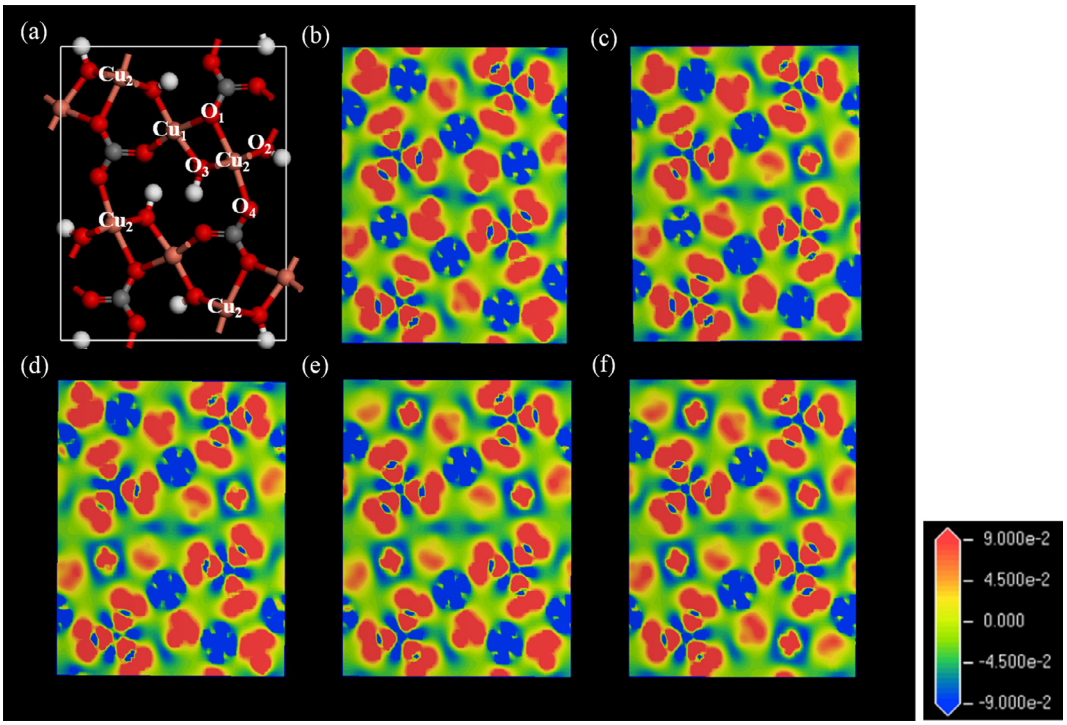

Fig. 4. The structure model (a), charge density difference of all the atoms for ($\bar{2}01$) plane of $Cu_2(OH)_2CO_3$ (b), $(Cu_{7/8}Zn_{1/8})_2(OH)_2CO_3$ (c), $(Cu_{6/8}Zn_{2/8})_2(OH)_2CO_3$ (d), $(Cu_{5/8}Zn_{3/8})_2(OH)_2CO_3$ (e) and $(Cu_{4/8}Zn_{4/8})_2(OH)_2CO_3$ (f) crystals.

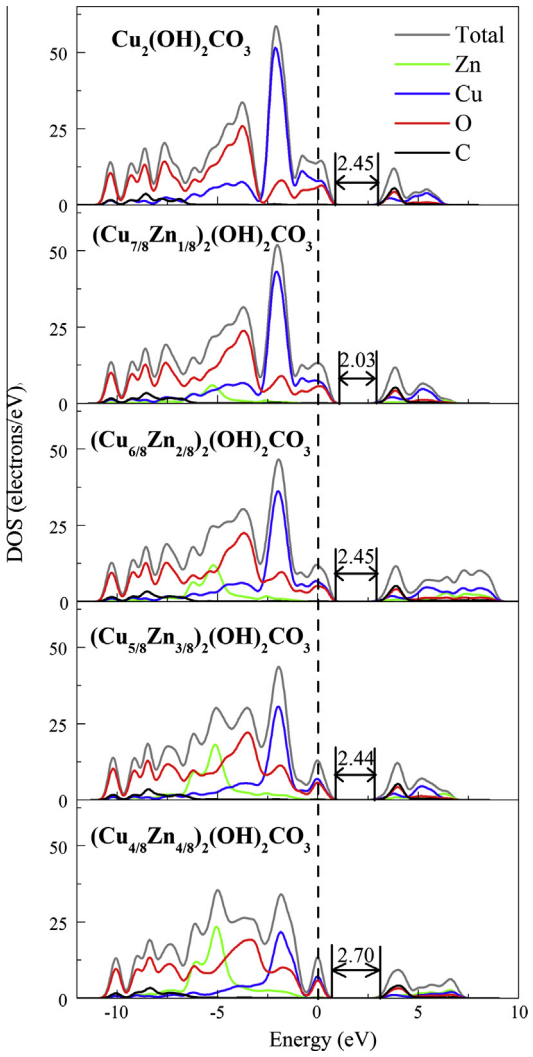

Fig. 5. The calculated total density of states (TDOS) of $(Cu_{1-x}Zn_x)_2(OH)_2CO_3$ with $x = 0$, 1/8, 2/8, 3/8 and 4/8.

Fig. 3) for different Zn doping contents which have significant influence on the charge density distribution. Besides, the cell volume of $(Cu_{6/8}Zn_{2/8})_2(OH)_2CO_3$, 352.124 Å^3, is larger than those of other Zn-doped compounds. Behrens et al. [11] have reported that the Jahn–Teller effect might be responsible for cell volume variation.

The average bond lengths of $(Cu_{1-x}Zn_x)_2(OH)_2CO_3$ are listed in Table 3 for comparison. It can be found that the average equatorial and apical bond lengths of Cu_1–O and Cu_2–O are 1.921, 2.689, 1.974 and 2.341 Å, respectively, in accordance with the experimental values [15,21]. The apical bond length of Cu_1–O is much longer than the equatorial bond length, whereas the difference between equatorial and apical bond lengths of Cu_2–O is smaller, which means Jahn–Teller distortion is particularly evident in the Cu_1 site. The average equatorial Zn–O bond lengths (2.041–2.063 Å) of Zn-doped $Cu_2(OH)_2CO_3$ are greater than Cu_1–O bond lengths (1.914–1.934 Å), which may be due to the larger ionic radius of Zn^{2+} than that of Cu^{2+}. It is interesting to note from Table 3 that the average apical bond lengths of Cu_1–O (2.670 Å) and Zn–O (2.131 Å) in $(Cu_{6/8}Zn_{2/8})_2(OH)_2CO_3$ are the shortest among $(Cu_{1-x}Zn_x)_2(OH)_2CO_3$ system, obtaining the weakest Jahn–Teller octahedral distortion. Moreover, as the most stable structure, $(Cu_{6/8}Zn_{2/8})_2(OH)_2CO_3$ inclines to the structural balance because of the same coordination environment between the first and second Zn atoms which results in the local structural equilibrium between the two Zn atoms.

3.3. Electronic properties

3.3.1. Population analysis

To understand interatomic bonding behaviors of $(Cu_{1-x}Zn_x)_2(OH)_2CO_3$ ($x = 0$, 1/8, 2/8, 3/8 and 4/8) crystals, the calculated Mulliken charges (e) for $(\bar{2}01)$ plane are shown in Table 4, which contains the equatorial MO_4 (M = Cu or Zn) planes of the MO_6 octahedral units as well as carbonate groups and hydroxyl groups [11,19]. For pure malachite, the net charge (0.83 e) of Cu_1 is a little smaller than that (0.86 e) of Cu_2, implying that the Cu_2–O bond possesses a stronger covalent bonding strength than Cu_1–O bond. For Zn-doped $Cu_2(OH)_2CO_3$, the net charges (1.37–1.24 e) of Zn are much larger than those of Cu_1 (0.77–0.67 e), resulting in the stronger covalent bonding strength of Zn–O bond. Meanwhile, the net charges of Zn are greater than those of Cu_2 atoms, and the net charges of O atoms are lower than the corresponding ones in pure malachite (Table 4). It is worth noting that with Zn content increasing, the net charges of Cu_1 and Zn exhibit a similar decreasing trend. In detail, the net charges of Cu_1 reduce from 0.77 to 0.67 e due to the obvious change of 4p state electrons, and the net charges of Zn decrease from 1.37 to 1.24 e as a result of a gradual increase of the 4s and 4p orbital electrons. Interestingly, when Zn substituting one Cu_2 atom, the 3d state electron of zinc increases to 9.98 e, then remains invariant with Zn content increasing. The 3d orbital of Zn behaves as a dominant core orbital in which the 9.98 e are nearly full-filled. In addition, it can be seen from Table 4 that the charges of O_2 and O_3 atoms originating from hydroxyl groups obtain more electrons than that of O_1 and O_4 atoms deriving from carbonate groups, suggesting that the M–O_2 (O_3) bonds possess more significant covalent character than M–O_1 (O_4) bonds.

In order to visualize the nature of the bonding character between Zn and adjacent O atoms, we have obtained valence charge density difference for $(\bar{2}01)$ plane of pure and Zn-doped malachite system in Fig. 4. The negative and positive values correspond to the ability to gain and lose electrons, respectively. The density difference maps indicate that O atom withdraws electrons from Cu_1 and Cu_2 atoms in pure $Cu_2(OH)_2CO_3$, which could be attributed to losing electrons of Cu 3d orbital. In comparison with malachite, the incorporation of Zn impurity results in an obvious change of 3d states. There exists the covalent bond feature between Zn and adjacent O atoms which is stronger than Cu_1–O atoms due to obvious overlap of electron clouds with a strong interaction. Therefore, Zn doping would induce a change of electronic structure in the Zn-doped $Cu_2(OH)_2CO_3$ system based on the alteration of electron cloud track for O atoms. In addition, the weaker covalent bond between Cu_1 and adjacent O atoms indicates that more electrons should transfer from Cu_1 to adjacent O atoms rather than the sharing of electrons as between Zn and adjacent O atoms. It is also expected that the carbonate groups are able to maintain the stable configurations and positions. The electrons of C transfer to the adjacent three O atoms, and C–O bonds are formed by the common electron cloud and exhibit a typical covalent character. The analysis results of Mulliken population are nicely supported by the change of electron density. Moreover, it can be observed from Fig. 4(c), O_2/O_3 obtains the fewer electrons than O_1/O_4, which is inconsistent with the above population analysis based on Table 4. It is caused by the hydroxyl ions slightly deviating from the $(\bar{2}01)$ plane after Zn doping in malachite.

The analysis results of average overlap populations for pure and Zn-doped malachite system are presented in Table 3 to further understand the bonding behavior among atoms. It is well known that a greater value of bond population represents a higher covalence level, while a value of zero is considered as an ideal ionic bond [37,38]. For pure $Cu_2(OH)_2CO_3$, the Mulliken bonding population of Cu_1–O and Cu_2–O are 0.25 and 0.26 e, respectively, suggesting that the covalent bonding characteristic of Cu_2–O should be

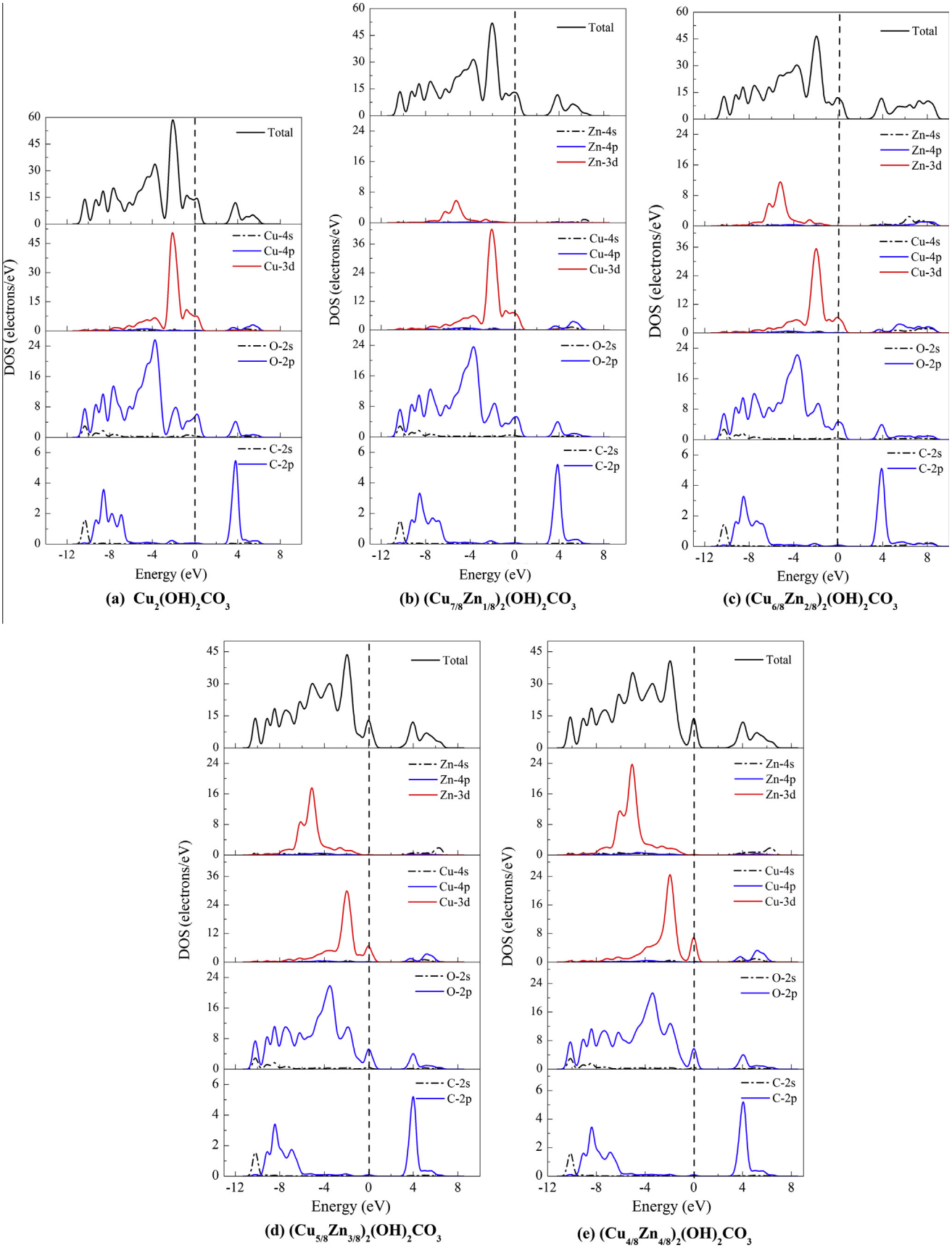

Fig. 6. Partial density of state (PDOS) of $(Cu_{1-x}Zn_x)_2(OH)_2CO_3$ with $x = 0$, 1/8, 2/8, 3/8 and 4/8.

slightly stronger than that of Cu_1–O. After Zn doping in the malachite, the Zn–O bonds (0.29–0.30 *e*) possess stronger covalent bonding strength than Cu_2–O and Cu_1–O bonds (0.26–0.28 *e*), which is coincident with the analysis results of atomic Mulliken charges and electron density difference. Hence, the covalent features gradually enhance in Zn-doped $Cu_2(OH)_2CO_3$ system with Zn contents increasing owing to the existence of more covalent Zn–O bonds, in good agreement with the experiment results [39,40].

3.3.2. Density of states (DOS) and Partial density of states (PDOS)

To further investigate the electronic structures of pure and Zn-doped malachite, the calculated density of states are shown in Fig. 5. It is worthwhile noting that the strong peaks are observed in the valence band (VB) for the above compounds with the different *x* values. The formed Cu orbital peaks are the highest peaks located around −2 eV in the VB. It is interesting to find that the peaks of Cu states are up to about 51.53, 43.13, 36.20, 30.06 and 21.69 electrons/eV for $(Cu_{1-x}Zn_x)_2(OH)_2CO_3$ ($x = 0$, 1/8, 2/8, 3/8 and 4/8), respectively, indicating that the contribution of Cu states gradually decreases with Zn content increasing. However, the formed peaks of Zn states located around −5 eV increase from 5.95 to 11.92, 18.15 and 23.42 electrons/eV, enhancing the more contributions in the valence band. The strength of chemical bond can be estimated from total density of states (TDOS) of $(Cu_{1-x}Zn_x)_2(OH)_2CO_3$ by comparing the energy levels of the bonding states located. From the point view of bonding energy, the Zn–O bonds are located at the lower energy level corresponding to a higher bonding strength; however, the Cu–O bonds extend to the higher energy level, and thus exhibit the weaker bonding strength. Besides, Fig. 5 also illustrates the energy band gaps of $Cu_2(OH)_2CO_3$ supercells with different Zn doping contents. The band gap reflects the energy gap of the valence band maximum (VBM) and the conduction band minimum (CBM) of the $(Cu_{1-x}Zn_x)_2(OH)_2CO_3$. It can be found that the band gap energy is in the range of 2.0–2.7 eV, which classifies the pure and Zn-doped malachite system as semiconductor materials.

The partial density of states (PDOS) of pure and Zn-doped malachite system are presented in Fig. 6. At the Fermi level, the density of states are 13.90, 13.16, 11.95, 12.97 and 13.43 electrons/eV, which are significantly dominated by the Cu 3d and O 2p states of $(Cu_{1-x}Zn_x)_2(OH)_2CO_3$, respectively. It is generally believed that a reduction in DOS at the Fermi level is benefit to the stability of a given structure [41,42]. That is, the lower the peak value of density of states is, the more the structure stability of system is. The valence electrons of $(Cu_{6/8}Zn_{2/8})_2(OH)_2CO_3$ exhibit the lowest peak value at the Fermi level, implying that it is the most stable structure, consistent with previous results of the formation energy. Furthermore, it can be found from Fig. 6(a)–(e), the valence bands of Zn-doped malachite are mainly composed of three energy parts. The highest energy region of VB (about from −2.5 eV to Fermi level) is mostly dominated by the Cu 3d and O 2p states, and the lowest energy region of VB (about from −11.2 to −8.7 eV) is composed of the hybridization of C 2p and O 2p states, forming carbonate groups. The intermediate energy states (about from −8.7 to −2.5 eV) is mostly originated from Zn 3d, O 2p and Cu 3d states. It can be seen clearly that the hybridization of Zn 3d and O 2p states becomes stronger with the concentration of Zn increasing, and is located farther to the Fermi level than that of Cu 3d and O 2p states, implying that the Zn–O bonds are stronger than the Cu–O bonds. In addition, the effect of p–d coupling on the electronic property of valence band is weaker in pure malachite than in Zn-doped malachite, because Cu 3d orbitals are more localized than Zn 3d orbitals. The whole conduction bands could be divided into two parts: the lower energy region between 2.7 and 4.8 eV and the higher energy level of conduction band from 4.8 to 7.5 eV. The former part, containing the bottom of conduction band, is chiefly contributed by C 2p and O 2p states, and the latter is mainly consisted of Cu 4p states, with slight contributions from Zn 4s and O 2p states.

4. Conclusions

In summary, we study the crystal structure, structural stability, bonding behavior, Mulliken charge and electronic structure of $(Cu_{1-x}Zn_x)_2(OH)_2CO_3$($x = 0$, 1/8, 2/8, 3/8 and 4/8) system by using density functional theory (DFT) within a plane-wave ultrasoft pseudopotential scheme. The key results are as follows:

(1) The obtained formation energies between 0.703 and 0.725 eV for Zn-doped malachite system indicate the formation of the doping should have a relative poor thermodynamic stability than pure malachite. $(Cu_{6/8}Zn_{2/8})_2(OH)_2CO_3$ is the most stable structure in thermodynamics due to the lowest formation energy of 0.703 eV. In addition, the supercells with Zn replacing Cu_2 sites always lead to the lowest formation energy, implying that Zn atoms should be preferential on the Cu_2 sites, in good accordance with the experimental results.

(2) The calculated structural parameters, including equilibrium lattice constants and average bond lengths, are consistent with the available experimental data. After the replacement of Zn, the supercells still belong to the monoclinic system. The average apical bond lengths of Cu_1–O and Cu_2–O are 2.689 and 2.341 Å, respectively, suggesting that the Jahn–Teller distortion is particularly evident in the Cu_1 site. For Zn-doped malachite system, the average equatorial Zn–O bond lengths (2.041–2.063 Å) of Zn-doped $Cu_2(OH)_2CO_3$ are greater than those of Cu_1–O (1.914–1.934 Å). Besides, the shortest bond lengths of Cu_1–O (2.670 Å) and Zn–O (2.131 Å) in $(Cu_{6/8}Zn_{2/8})_2(OH)_2CO_3$ exhibit the weakest Jahn–Teller distortion.

(3) The analysis results of Mulliken charge, bond populations and charge density difference demonstrate that there exist the sequence of Zn–O > Cu_2–O > Cu_1–O covalent bonds, and the covalent features gradually enhance in Zn-doped $Cu_2(OH)_2CO_3$ system with the increasing incorporation amount of Zn dopant.

(4) The calculated results of density of states indicate that the hybridization of Zn 3d and O 2p states becomes stronger with the Zn concentration increasing, and the covalent feature of Zn–O bonds are much stronger than Cu–O bonds. The lowest peak value of valence electrons of $(Cu_{6/8}Zn_{2/8})_2(OH)_2CO_3$ at the Fermi level further implies the most stable structure, consistent with previous results of formation energy. Moreover, the band gaps for $(Cu_{1-x}Zn_x)_2(OH)_2CO_3$ ($x = 0$, 1/8, 2/8, 3/8 and 4/8) are 2.45, 2.03, 2.45, 2.44 and 2.7 eV, respectively, determining that $(Cu_{1-x}Zn_x)_2(OH)_2CO_3$ system belong to the characteristic of semiconductor materials.

Acknowledgements

This work is supported by the National Natural Science Foundation of China (21106092) and the National Basic Research Program of China (2012CB723105).

References

[1] M. Behrens, F. Studt, I. Kasatkin, S. Kühl, M. Hävecker, F. Abild-Pedersen, S. Zander, F. Girgsdies, P. Kurr, B.-L. Kniep, M. Tovar, R.W. Fischer, J.K. Nørskov, R. Schlögl, Science 336 (2012) 893.

[2] J.P. Greeley, Science 336 (2012) 810.
[3] P.L. Hansen, J.B. Wagner, S. Helveg, J.R. Rostrup-Nielsen, B.S. Clausen, H. Topsøe, Science 295 (2002) 2053.
[4] S. Zander, E.L. Kunkes, M.E. Schuster, J. Schumann, G. Weinberg, D. Teschner, N. Jacobsen, R. Schlogl, M. Behrens, Angew. Chem. Int. Ed. 52 (2013) 6536.
[5] C. Baltes, S. Vukojević, F. Schüth, J. Catal. 258 (2008) 334.
[6] A. Budiman, M. Ridwan, S.M. Kim, J.-W. Choi, C.W. Yoon, J.-M. Ha, D.J. Suh, Y.-W. Suh, Appl. Catal. A: Gen. 462–463 (2013) 220.
[7] M. Behrens, I. Kasatkin, S. Kuhl, G. Weinberg, Chem. Mater. 22 (2010) 386.
[8] M. Behrens, S. Kissner, F. Girsgdies, I. Kasatkin, F. Hermerschmidt, K. Mette, H. Ruland, M. Muhler, R. Schlogl, Chem. Commun. 47 (2011) 1701.
[9] M. Behrens, F. Girgsdies, A. Trunschke, R. Schlogl, Eur. J. Inorg. Chem. (2009) 1347.
[10] M. Behrens, J. Catal. 267 (2009) 24.
[11] M. Behrens, F. Girgsdies, A. Trunschke, R. Schlögl, Eur. J. Inorg. Chem. 2009 (2009) 1347.
[12] S. Klokishner, M. Behrens, O. Reu, G. Tzolova-Muller, F. Girgsdies, A. Trunschke, R. Schlogl, J. Phys. Chem. A 115 (2011) 9954.
[13] I.B. Bersuker, The Jahn–Teller Effect, Cambridge University Press, Cambridge, 2006.
[14] M. Merlini, N. Perchiazzi, M. Hanfland, A. Bossak, Acta Crystallogr. B 68 (2012) 266.
[15] M. Behrens, F. Girgsdies, Z. Anorg, Allg. Chem. 636 (2010) 919.
[16] F. Girgsdies, M. Behrens, Acta Crystallogr. B 68 (2012) 107.
[17] G.J. Millar, I.H. Holm, P.J. Uwins, J. Drennan, J. Chem. Soc, Faraday Trans. 94 (1998) 593.
[18] B. Bems, M. Schur, A. Dassenoy, H. Junkes, D. Herein, R. Schlögl, Chem.-Eur. J. 9 (2003) 2039.
[19] S. Lebernegg, A.A. Tsirlin, O. Janson, H. Rosner, Phys. Rev. B 88 (2013) 224406.
[20] P. Süsse, Acta Crystallogr. 22 (1967) 146.
[21] F. Zigan, W. Joswig, H.D. Schuster, S.A. Mason, Z. Kristallogr. 145 (1977) 412.
[22] A.F. Wells, Acta Crystallogr. 4 (1951) 200.
[23] S.J. Clark, M.D. Segall, C.J. Pickard, P.J. Hasnip, M.I. Probert, K. Refson, M.C. Payne, Z. Kristallogr. 220 (2005) 567.
[24] M. Segall, P.J. Lindan, M. Probert, C. Pickard, P. Hasnip, S. Clark, M. Payne, J. Phys.: Condens. Matter 14 (2002) 2717.
[25] D. Vanderbilt, Phys. Rev. B 41 (1990) 7892.
[26] J.P. Perdew, A. Zunger, Phys. Rev. B 23 (1981) 5048.
[27] H.H. Kim, J.W. Yang, S.B. Jo, B. Kang, S.K. Lee, H. Bong, G. Lee, K.S. Kim, K. Cho, ACS Nano 7 (2013) 1155.
[28] C. Di Valentin, G. Pacchioni, A. Selloni, Chem. Mater. 17 (2005) 6656.
[29] K. Sumida, D. Stuck, L. Mino, J.D. Chai, E.D. Bloch, O. Zavorotynska, L.J. Murray, M. Dinca, S. Chavan, S. Bordiga, M. Head-Gordon, J.R. Long, J. Am. Chem. Soc. 135 (2013) 1083.
[30] N. Perchiazzi, Z. Kristallogr. 2006 (2006) 505.
[31] A.I. Khan, D. O'Hare, J. Mater. Chem. 12 (2002) 3191.
[32] D.G. Costa, A.B. Rocha, W.F. Souza, S.S.X. Chiaro, A.A. Leitão, J. Phys. Chem. C 112 (2008) 10681.
[33] A. Vaccari, Catal. Today 41 (1998) 53.
[34] Z.M. Ni, P. Yao, X.M. Liu, Q.Q. Wang, Q. Xu, Chem. J. Chinese U. 31 (2010) 2438.
[35] H. Yan, M. Wei, J. Ma, D.G. Evans, X. Duan, J. Phys. Chem. A 114 (2010) 7369.
[36] G.G.C. Arizaga, K.G. Satyanarayana, F. Wypych, Solid State Ionics 178 (2007) 1143.
[37] M. Segall, R. Shah, C. Pickard, M. Payne, Phys. Rev. B 54 (1996) 16317.
[38] X.C. Zhang, C.M. Fan, Y.W. Wang, Y.F. Wang, Z.H. Liang, P.D. Han, Comp. Mater. Sci. 71 (2013) 135.
[39] P. Porta, G. Fierro, M.L. Jacano, G. Moretti, Catal. Today 2 (1988) 675.
[40] P. Porta, S. De Rossi, G. Ferraris, M. Lo, J. Catal. 109 (1988) 367.
[41] C.L. Fu, X. Wang, Y.Y. Ye, K.M. Ho, Intermetallics 7 (1999) 179.
[42] P. Chen, D.L. Li, J.X. Yi, L. Wen, B.Y. Tang, L.M. Peng, W.J. Ding, Solid State Sci. 11 (2009) 2156.